

# Following in Operando the Structure Evolution-Induced Degradation in Printed Organic Solar Cells with Nonfullerene Small Molecule Acceptor

Kerstin S. Wienhold, Wei Chen, Shanshan Yin, Renjun Guo, Matthias Schwartzkopf, Stephan V. Roth, and Peter Müller-Buschbaum\*

Understanding the degradation mechanisms of printed bulk-heterojunction (BHJ) organic solar cells during operation is essential to achieve long-term stability and realize real-world applications of organic photovoltaics. Herein, the degradation of printed organic solar cells based on the conjugated benzodithiophene polymer PBDB-T-SF and the nonfullerene small molecule acceptor IT-4F with 0.25 vol% 1,8-diiodooctane (DIO) solvent additive is studied in operando for two different donor:acceptor ratios. The inner nano-morphology is analyzed with grazing incidence small angle X-ray scattering (GISAXS), and current–voltage ( $I$ – $V$ ) characteristics are probed simultaneously. Irrespective of the mixing ratio, degradation occurs by the same degradation mechanism. A decrease in the short-circuit current density ( $J_{SC}$ ) is identified to be the determining factor for the decline of the power conversion efficiency. The decrease in  $J_{SC}$  is induced by a reduction of the relative interface area between the conjugated polymer and the small molecule acceptor in the BHJ structure, resembling the morphological degradation of the active layer.

## 1. Introduction

Organic solar cells show great potential as a renewable energy source, and power conversion efficiencies (PCEs) above 16% were demonstrated for lab-scale devices.<sup>[1,2]</sup> However, on the way to marketability, the long-term stability of these devices has to be improved, and a large-scale fabrication process has to be developed. To overcome the challenge of upscaling the thin-film deposition, promising techniques, such as spraying, inkjet printing, and meniscus-guided slot-die coating, are introduced in the field of organic photovoltaics.<sup>[3–12]</sup> Even though the stability of organic solar cells could be improved successfully by the synthesis of new materials,<sup>[13–15]</sup> end-group and side-chain modification,<sup>[16]</sup> or the development of an inverted device structure,<sup>[17–21]</sup> the poor long-term stability of


most high-efficiency materials has to be further improved for a commercial breakthrough.<sup>[22–26]</sup> Therefore, understanding the degradation mechanism of printed bulk-heterojunction (BHJ) photovoltaics is essential to realize the production of large-area organic solar cells with outstanding PCE and excellent long-term stability. The chemical degradation of organic solar cells in the presence of water or oxygen has been studied for many materials and can be avoided by proper encapsulation of the devices.<sup>[19,27]</sup> However, physical degradation with morphological changes in the active layer occurs even in the absence of reactive molecules as shown for several materials.<sup>[22–24]</sup> So far, two major pathways of the morphological degradation were identified: Starting from an optimized morphology of the BHJ, either a demixing-induced coarsening of the domains or mixing-induced shrinkage of the domains was identified.<sup>[22–24]</sup> Domain coarsening in combination with an increase in distances between neighboring domains resulted in a decrease in the short-circuit current density ( $J_{SC}$ ) during device degradation as first identified for the model system poly(3-hexylthiophene) (P3HT) and phenyl-C61-butyric acid methyl ester (PCBM).<sup>[22]</sup> Domain shrinkage caused a loss in connectivity, thereby inducing dead ends for charge carriers, and resulted in a fill factor (FF)-driven device degradation as found in the case of poly[2,1,3-benzothiadiazole-4,7-diyl [4,4-bis[2-ethylhexyl]-4H-cyclopenta[2,1-b:3,4-b'] dithiophene-2,6-diyl]], (PCPDTBT) and phenyl-C71-butyric acid methyl ester

K. S. Wienhold, W. Chen, S. Yin, R. Guo, Prof. P. Müller-Buschbaum  
Physik-Department  
Lehrstuhl für Funktionelle Materialien  
Technische Universität München  
James-Franck-Str. 1, 85748 Garching, Germany  
E-mail: muellerb@ph.tum.de

Dr. M. Schwartzkopf, Prof. S. V. Roth  
DESY  
Notkestraße 85, 22607 Hamburg, Germany

Prof. S. V. Roth  
Department of Fibre and Polymer Technology  
KTH Royal Institute of Technology  
Teknikringen 56-58, SE-100 44 Stockholm, Sweden

Prof. P. Müller-Buschbaum  
Heinz Maier-Leibnitz-Zentrum  
Technische Universität München  
Lichtenbergstr. 1, 85748 Garching, Germany

 The ORCID identification number(s) for the author(s) of this article can be found under <https://doi.org/10.1002/solr.202000251>.

© 2020 The Authors. Published by WILEY-VCH Verlag GmbH & Co. KGaA, Weinheim. This is an open access article under the terms of the Creative Commons Attribution License, which permits use, distribution and reproduction in any medium, provided the original work is properly cited.

DOI: 10.1002/solr.202000251

(PC<sub>71</sub>BM).<sup>[24]</sup> Recently, the use of solvent additives was shown to cause a change in the morphological degradation as demonstrated for the high-efficiency low-bandgap benzodithiophene copolymer PTB7-Th and PC<sub>71</sub>BM.<sup>[23]</sup> However, these pioneering studies were all focusing on active layers prepared with spin-coating.

In this work, the physical degradation mechanism of meniscus-guided slot-die-coated organic solar cells is studied for the first time. The morphological evolution of organic solar cells based on the conjugated polymer poly[(2,6-(4,8-bis(5-(2-ethylhexylthio)-4-fluorothiophen-2-yl)-benzo[1,2-b:4,5-b']dithiophene))-*alt*-(5,5-(1',3'-di-2-thienyl-5',7'-bis(2-ethylhexyl)benzo[1',2'-c:4',5'-c']dithiophene-4,8-dione))], denoted PBDB-T-SF, and the nonfullerene small molecule acceptor 3,9-bis(2-methylene-((3-(1,1-dicyanomethylene)-6,7-difluoro)-indanone))-5,5,11,11-tetrakis(4-hexylphenyl)-dithieno[2,3-d:2',3'-d']-s-indaceno[1,2-b:5,6-b']dithiophene, denoted IT-4F, is probed in operando. Thus, we address, for the first time, the morphology degradation of a nonfullerene small molecule acceptor-based high efficiency-type solar cell, which can achieve a champion PCE of 13%.<sup>[28,29]</sup> Organic solar cells processed with two different donor:acceptor mixing ratios (1:1 and 1:2) are studied in operando with grazing incidence small angle X-ray scattering (GISAXS)<sup>[30–32]</sup> to follow the evolution of morphology during operation. Simultaneously, current–voltage (*I*–*V*) curves are measured to extract the *J*<sub>SC</sub>, open-circuit voltage (*V*<sub>OC</sub>), FF, and PCE and to correlate these device parameters with morphological changes observed with GISAXS. To enable such correlation, a theoretical model is used to predict the degradation of the *J*<sub>SC</sub> based on the probed active layer morphology, because *J*<sub>SC</sub> is identified to be the determining factor in device degradation. For all devices investigated in this work, a reduction of the interface-to-volume ratio in the BHJ layer provokes a decline of *J*<sub>SC</sub> with operation time.

## 2. Results and Discussion

The morphology degradation of PBDB-T-SF:IT-4F-based organic solar cells printed with two different donor:acceptor ratios is studied in operando under illumination from a solar simulator. To exclude chemical degradation pathways within this study, the experiments are performed under moderate vacuum conditions (10<sup>−2</sup> mbar, see experimental chamber in Figure S1, Supporting Information). Therefore, we avoid possible reactions between the active layer materials and oxygen, such as the irreversible photochemical formation of carbonyl and carboxylic groups, which act as electron traps or the reversible p-doping of the active layer with oxygen, provoking the formation of immobilized superoxide anions.<sup>[33]</sup> In addition, a possible degradation of the aluminum electrodes or the active layer by air humidity<sup>[34–37]</sup> is ruled out under these conditions. A potential decomposition of the nonfullerene small molecule acceptor by the photocatalytic activity of ZnO under illumination with UV light<sup>[38]</sup> is ruled out, as the light of the solar simulator passes through a quartz glass window, which is not transparent to this wavelength range. As current density–voltage (*J*–*V*) characteristics depend on the light intensity,<sup>[39,40]</sup> this parameter is kept stable during the measurement (AM 1.5 illumination, 100 mW cm<sup>−2</sup>). Moreover, the chamber is cooled to 15 °C to avoid temperature-induced changes of the morphology or the solar cell performance.<sup>[41–43]</sup>

As proved in earlier studies,<sup>[22–24]</sup> morphology degradation is well studied in operando with a simultaneous measurement of GISAXS and *J*–*V* characteristics. To obtain statistical information, four organic solar cells are connected in parallel to measure average *J*–*V* characteristics. In addition, in the GISAXS experiment, the X-ray beam is aligned to impinge the sample as a small line, which gives morphological information about the four organic solar cells simultaneously. For GISAXS, we select an incidence angle (of 0.4°) well above the critical angles of the involved materials, such as PBDB-T-SF and IT-4F, to probe information from the full thickness and analyze the inner nano-structure of the active layer.<sup>[31,44]</sup> The grazing incidence geometry allows analyzing a larger sample area with high statistical significance and to measure thin films with a layer thickness on the order of 100 nm, which is assumed to be the ideal thickness regime for organic solar cells.<sup>[28]</sup>

### 2.1. Degradation of Organic Solar Cells with 1:1 and 1:2 Donor:Acceptor Ratio

The 2D GISAXS data of printed organic solar cells with a 1:1 and 1:2 donor:acceptor ratio show the significant change of morphology during operation (Figure S2 and S3, Supporting Information). Within the first 30 min, a fast and distinct structure evolution is observed. At longer illumination times, the change of the morphology decelerates and almost stabilizes but does not fully stop within the time span of the in operando experiment. For 2D GISAXS data analysis, horizontal line cuts (Figure 1a,e) are carried out at the strongest scattering contribution, the critical angle (Yoneda region) of PBDB-T-SF, which is calculated to be 0.12° for the used X-ray energy of 11.65 keV. To obtain the average polymer domain sizes in the active layer, these horizontal line cuts are modeled. The used model is based on the effective interface approximation (EIA) of the distorted wave Born approximation (DWBA).<sup>[45,46]</sup> To consider the local monodisperse approximation (LMA), the overall scattering intensity is defined as an incoherent superposition of scattering intensities originating from individual polymer domains in the thin film. The GISAXS data are modeled with three cylindrical substructures, which is a well-established approach to characterize the morphology of thin polymer films.<sup>[47–49]</sup> The respective cylinders are assumed to be pure polymer domains.<sup>[22]</sup> In Figure 1a,e, horizontal line cuts of the 2D GISAXS data (black dots) for printed organic solar cells based on a 1:1 and 1:2 donor:acceptor ratio and the corresponding modeling results (red lines) are shown for different operation times (from bottom to top). For organic solar cells based on a 1:1 donor:acceptor ratio, the average structure sizes of polymer domains increase under operation (Figure 1b–d). The largest structure (Figure 1b) grows from (80 ± 2) nm to (98 ± 2) nm, whereas the medium structure (Figure 1c) grows from (30 ± 1) nm to (39 ± 1) nm and the smallest structure (Figure 1d) from (10.0 ± 0.5) nm to (17.0 ± 0.5) nm. The corresponding distances are (200 ± 10) nm, (130 ± 10) nm, and (50 ± 5) nm and do not change significantly within the time span of the experiment. For organic solar cells based on a 1:2 donor:acceptor ratio, the largest domain structure (Figure 1f) grows from (90 ± 2) nm to (117 ± 2) nm. The medium structure size (Figure 1g) is about (29 ± 1) nm at the start of the operation and grows to (36 ± 1) nm during operation, which is similar to

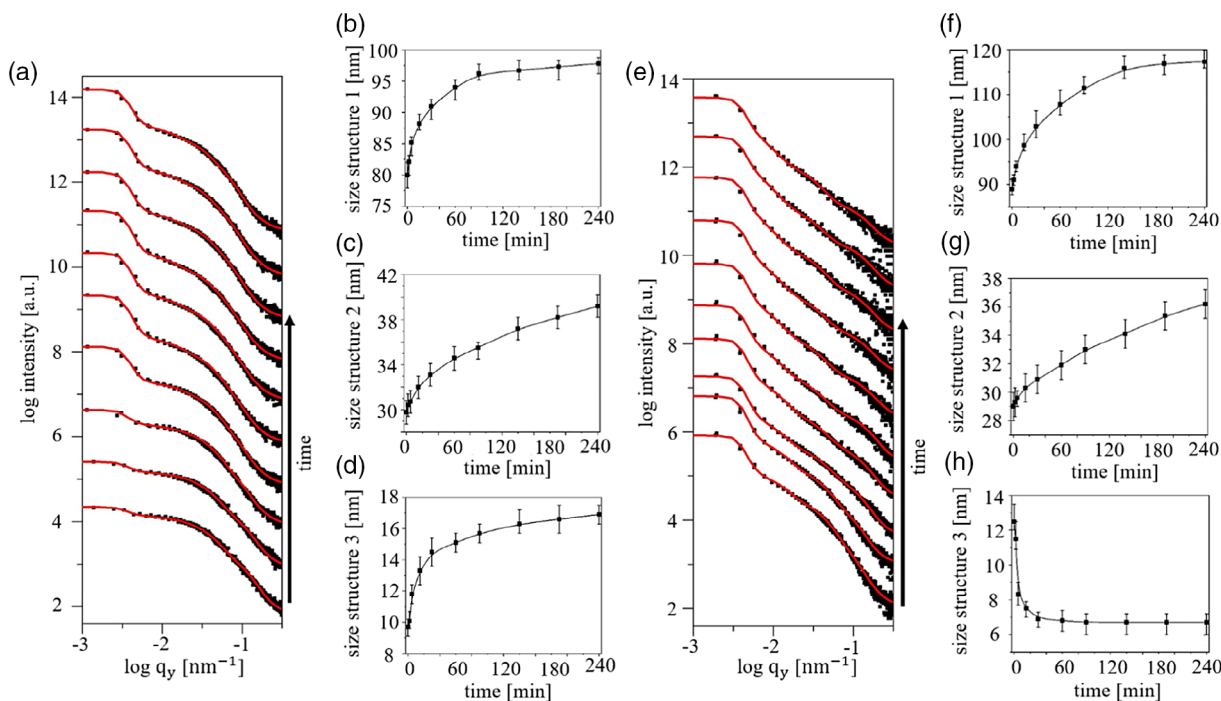


**Figure 1.** Temporal evolution of the morphology of printed organic solar cells based on a a–d) 1:1 PBDB-T-SF:IT-4F ratio and e–h) 1:2 ratio. a,e) Horizontal line cuts of the 2D GISAXS data (black dots) and modeling results (red lines) by applying a model based on the DWBA and the LMA are shown for different time steps of operation (0, 2, 5, 15, 30, 60, 90, 140, 190, and 240 min, from bottom to top). Parameters determined from the GISAXS modeling are the average domain sizes for the b,f) largest, c,g) medium, and d,h) smallest polymer domains. The error bars give a range in which the fit still describes the scattering data. The solid black lines (in b–d) and (f–h)) are guides to the eye.

the findings obtained for the device based on a 1:1 donor:acceptor ratio. In contrast, the size of the smallest polymer domains (Figure 1h) is reduced from  $(12.5 \pm 1.0)$  nm to  $(6.5 \pm 1.0)$  nm, which is a trend opposite to what is found in the 1:1 donor:acceptor ratio device. The corresponding distances are  $(200 \pm 10)$  nm,  $(100 \pm 10)$  nm, and  $(40 \pm 5)$  nm and do not alter during the operation.

The observed structural growth under operation of a printed organic solar cell based on a 1:1 ratio of PBDB-T-SF:IT-4F shares a limited similarity to findings from previous studies performed on spin-coated P3HT:PCBM devices with a 1:1 donor:acceptor ratio.<sup>[22]</sup> However, for such fullerene-based organic solar cells, the increase in domain sizes and also the average distance between medium-sized domains increased significantly under illumination. In active layers prepared with solvent additive, so far, a domain shrinkage was reported as a morphology degradation mechanism instead of a domain coarsening.<sup>[23]</sup> Therefore, for the PBDB-T-SF:IT-4F solar cells of this study being manufactured with 0.25 vol% 1,8-diiodooctane (DIO) as solvent additive,<sup>[50]</sup> the observed domain coarsening is unexpected.

The observed morphological degradation in PBDB-T-SF:IT-4F solar cells based on a 1:2 ratio shares no similarity with previous studies performed on organic solar cells with an excess of acceptor. Schaffer et al. observed a decrease in the medium and smallest domain sizes under illumination of a spin-coated PCPDTBT:PCBM-based organic solar cell with a 1:2.7 donor:acceptor ratio prepared with solvent additive.<sup>[24]</sup> For a spin-coated

PTB7-Th:PCBM-based device with a donor:acceptor of 1:1.5, Yang et al. observed decreasing average structure sizes for devices processed with solvent additive.<sup>[23]</sup> In both systems, the FF and not the  $J_{SC}$  were detrimental to the device failure. The amount of residual solvent additive was determined by the relative scattering intensity at the critical angle of the respective compound.<sup>[23,24]</sup> A loss in solvent additive was found responsible for the domain shrinkage in previous works, which is not observed in this study (Figure S5, Supporting Information). This is favorable, as DIO was found to enhance the device performance of printed PBDB-T-SF:IT-4F-based organic solar cells by provoking the formation of small polymer domains in the BHJ layer.<sup>[50]</sup>

In contrast to previous studies, structure coarsening without altering the average distances between polymer domains is found to be the crucial factor for device failure in our work. We assume this is due to different chemical structures of the active materials, which provoke different interactions of the donor and acceptor molecules with surrounding molecules. During device degradation, rearrangement of the polymer can occur provoking microstructure evolution and charge trapping. However, the aggregation of the nonfullerene small molecule acceptor is diffusion-limited and, therefore, has a stabilizing effect on the BHJ morphology.<sup>[51]</sup> In addition, in this study, the correlated roughness determined by vertical line cuts of the 2D GISAXS data is only poorly developed and changes only slightly or even decreases under illumination (Figure S4, Supporting Information), which differs from previous studies, which observed a significant increase in correlated roughness for solar

cells processed with DIO.<sup>[23]</sup> Thus, the different degradation mechanism found for PBDB-T-SF:IT-4F solar cells as compared with other systems is attributed to the different mobility and interactions of the involved donor and acceptor materials.

## 2.2. Modeling the Degradation of the Short-Circuit Current Density

From the three different characteristic structure sizes determined in the GISAXS data analysis, the size of the medium substructure, which is about some tens of nanometer, is expected to be the crucial factor, as it is close to the scale of typical exciton diffusion lengths determined for several organic solar cell materials.<sup>[52–56]</sup> For slot-die-coated active layers based on PBDB-T-SF:IT-4F, the size of the medium substructure is about 30 nm. The morphology observed with atomic force microscopy (AFM) for spin-coated active layers is similar to the morphology observed for slot-die-coated PBDB-T-SF:IT-4F films even though the largest structure was not reported in the previous study.<sup>[28]</sup>

To correlate the morphological changes obtained from the scattering experiment with the solar cell performance,  $I$ - $V$  curves are measured simultaneously, and the characteristic device parameters are extracted. The initial parameters are given in Table S1, Supporting Information. **Figure 2a,c** shows the temporal evolution of the normalized device parameters, namely, the PCE,  $J_{SC}$ ,  $V_{OC}$ , and FF of printed organic solar cells based on

a 1:1 and a 1:2 donor:acceptor ratio within the first 4 h of illumination. The degradation of  $J_{SC}$  is identified to be the determining factor for the decay of the solar cell performance, as the device parameters  $V_{OC}$  and FF stabilize after 30 min and the relative values do not drop below 0.91 for the  $V_{OC}$  and 0.86 for the FF within the timescale of the experiment. Based on the knowledge from earlier studies of P3HT:PCBM solar cells, the significant reduction of the normalized  $J_{SC}$  to 0.76 for a 1:1 and 0.80 for a 1:2 donor:acceptor ratio is expected to result from a structure coarsening and a related reduction of the interface-to-volume ratio between donor and acceptor. As exciton splitting takes place at the interface, the probability of exciton dissociation into free charge carriers depends critically on the interface between donor and acceptor.<sup>[57,58]</sup> **Figure 3** shows the structure coarsening and reduction of interface-to-volume ratio in the BHJ during operation. In our model approach, in agreement with the model described by Schaffer et al.<sup>[22]</sup> it is assumed that only the medium-sized domains significantly contribute to the solar cell performance, as typical exciton diffusion lengths are in a similar range. In accordance with the model applied to describe the scattering data, polymer domains are described as cylinders (Figure 3a,c). In the model, a photon is absorbed by a polymer molecule within a cylindrical shaped domain, and an exciton is generated, which moves to the donor:acceptor interface where dissociation into free charge carriers occurs.<sup>[59,60]</sup> The probability for this process depends on the relative interface area between the polymer and the acceptor,

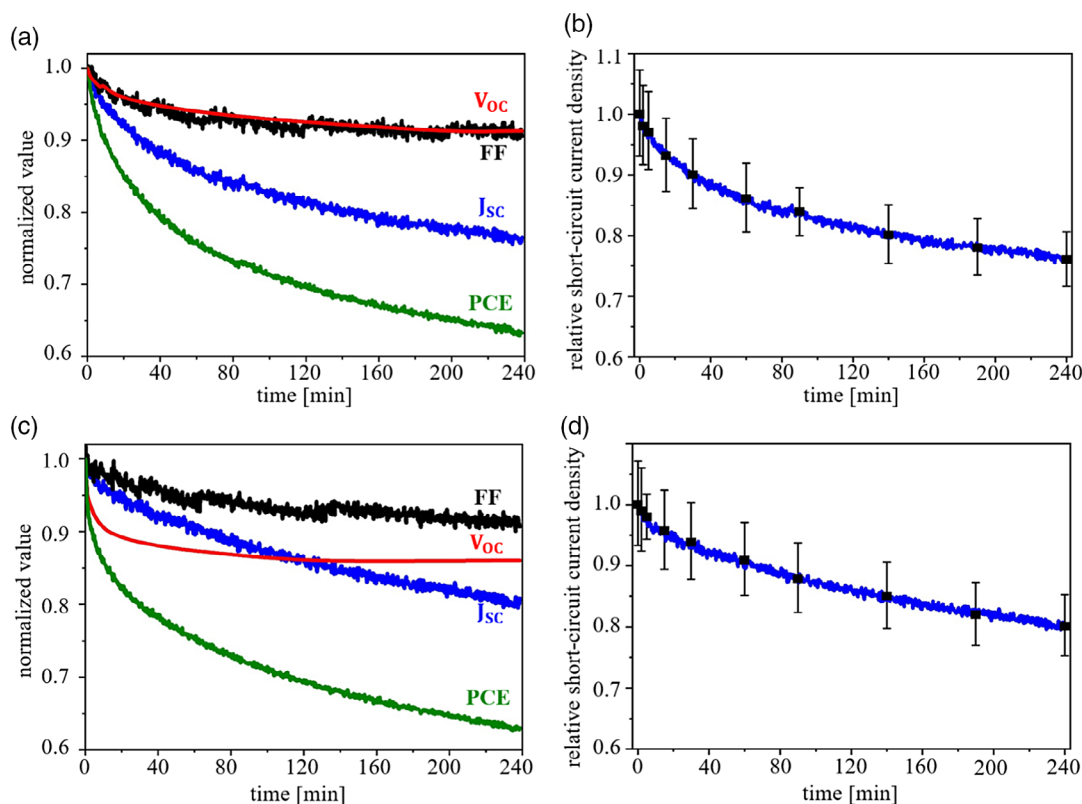


**Figure 2.** Degradation of normalized device parameters during operation for a printed organic solar cell based on a a,b) 1:1 and c,d) 1:2 donor:acceptor ratio of PBDB-T-SF:IT-4F in terms of a,c) PCE (green),  $J_{SC}$  (blue),  $V_{OC}$  (red), and FF (black). b,d) Comparison of the measured (blue) and theoretically predicted  $J_{SC}$  (black dots) using a model as explained in the text. The error bars arise from the GISAXS modeling error.

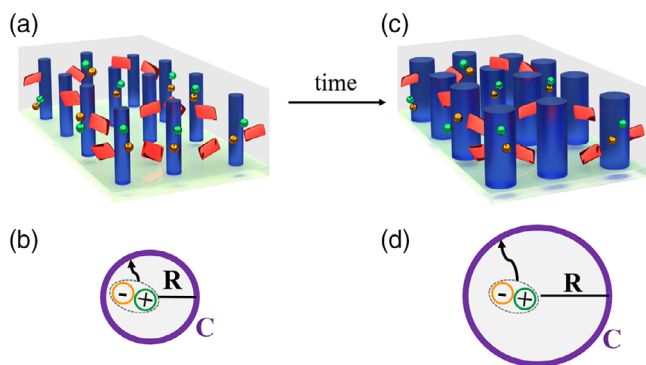


**Figure 3.** Schematic of the morphology evolution in the active layer during operation as assumed in the model with only a small fraction of acceptor molecules shown for clarity of the presentation. a) At the start of the operation, a BHJ structure with small polymer domains (blue cylinders) and small molecule acceptor domains (red cuboids) is observed. b) A cross section of a polymer cylinder with a small radius is shown. A high interface-to-volume ratio facilitates exciton dissociation into free charge carriers at the donor–acceptor interface. The electron (orange) and the electron hole (green) move toward the electrodes and a high  $J_{SC}$  is measured experimentally. The relative interface area is given by the circumference (purple) of the cylinder per cross-sectional area. c) Under illumination, a growth of polymer domains occurs. d) In the cross section, a reduction of interface (purple) between donor and acceptor is observed provoking a reduction of exciton dissociation probability. In a polymer cylinder with large radius, the interface-to-volume ratio is reduced provoking a reduction of exciton dissociation probability and  $J_{SC}$ .

which is defined as the interface-to-volume ratio of the polymer cylinder. Excitons that move along the length of the cylinder will undergo recombination before reaching the interface and do not contribute to the  $J_{SC}$ . Therefore, the photocurrent is independent of the length of the cylinder, and a consideration of the cylinder cross section is sufficient to explain the evolution of the relative  $J_{SC}$ . The probability of exciton dissociation and generation of photocurrent depends on the relative interface area and, respectively, on the circumference of the cylinder (Figure 3b,d). Equation (1) is based on a model developed by Schaffer et al. to predict the degradation of the normalized  $J_{SC}$  in a P3HT:PCBM-based spin-coated organic solar cell during operation.<sup>[22]</sup> Schaffer et al. described the degradation of short-circuit current density in P3HT:PCBM-based photovoltaics to originate from a reduction of the active area per unit cell area. Therefore, the geometrical factor to describe the evolution of morphology is given by the cylinder size and the average interdomain distances. The crucial factor for device failure of P3HT:PCBM-based solar cells was the significant increase in the average domain distances, which provoked an increase in the unit cell area and, therefore, reduced the ratio of active area per unit cell area even though the average polymer domain sizes increased moderately. However, for PBDB-T-SF:IT-4F-based organic solar cells, the average distances and, thus, the unit cell area are stable during the experiment. As a consequence, we develop a new model to describe the degradation of PBDB-T-SF:IT-4F-based solar cells, which describes the relationship between the normalized  $J_{SC}$  and the relative circumference  $C$  (defined as the circumference of the cylinder normalized on the cross-sectional area).  $Q$  is the

elementary charge,  $I$  refers to the light intensity, and  $p$  is the probability that a photon absorbed in the polymer domain contributes to the photocurrent. The light intensity  $I$  is stable during the in operando measurement. As chemical degradation pathways are ruled out by the measurement conditions, chemical properties of the active layer do not alter during the experiment for which reason  $p$  is assumed to be constant. In this model approach, structure parameters  $R$  (medium cylinder radii) are extracted from the GISAXS data modeling (Figure 1c,g).

$$J_{sc}^{norm}(t) = \frac{J_{sc}(t)}{J_{sc}(0)} = \frac{p \cdot Q \cdot I \cdot C(t)}{p \cdot Q \cdot I \cdot C(0)} = \frac{\frac{2\pi R(t)}{R(t)^2 \pi}}{\frac{2\pi R(0)}{R(0)^2 \pi}} = \frac{R(0)}{R(t)} \quad (1)$$

Figure 2b,d shows the evolution of the normalized  $J_{SC}$  extracted from the  $J$ – $V$  curves (blue) in comparison with the theoretically predicated value applying the model from Equation (1) (black dots). The error bars are estimated by calculating the theoretically predicted  $J_{SC}$  (Equation (1)) for the upper and lower domain size limit as determined in the GISAXS data modeling (Figure 1c,g). Model and experiment are in excellent agreement. Therefore, the decrease in the interface-to-volume ratio is identified to be the determining factor for the significant degradation of the  $J_{SC}$  during operation. The reduction of the relative  $J_{SC}$  to 0.76 for a 1:1 or 0.80 for a 1:2 donor:acceptor ratio provokes a decline of the normalized PCE to 0.63.

### 3. Conclusion

In the in operando study, we compare printed organic solar cells with two different donor:acceptor ratios of 1:1 and 1:2. Irrespective of the mixing ratio, degradation occurs by the same degradation mechanism, and a decrease in the  $J_{SC}$  is identified to be the determining factor for the decline of the PCE. With GISAXS, a growth of polymer domains is observed, whereas the domain distances remain unchanged, which causes a reduction of the interface-to-volume ratio in the BHJ. Thereby the probability of exciton dissociation is lowered. The observed decline of the  $J_{SC}$  correlates very well with the calculated current based on the changed nanoscale BHJ structure. Thus, the morphology degradation is leading to the device failure.

The degradation mechanism observed for printed PBDB-T-SF:IT-4F-based devices differs from previous studies on spin-coated fullerene-based organic solar cells. Therefore, new materials should be studied in operando, as knowledge gained from one material system might not simply be transferred to other materials or processing conditions. The presented results give insight into the degradation of meniscus-guided slot-die-coated organic solar cells and are a first step toward the development of long-term stable organic photovoltaics.

### 4. Experimental Section

**Device Fabrication:** In this work, organic solar cells with an inverted geometry (glass/indium tin oxide (ITO)/BHJ/MoO<sub>3</sub>/Al) were fabricated. The conjugated polymer poly[(2,6-(4,8-bis(5-(2-ethylhexylthio)-4-fluorothiophen-2-yl)-benzo[1,2-b:4,5-b']dithiophene))-alt-(5,5-(1',3'-di-2-thienyl)-5',7'-bis(2-ethylhexyl)benzo[1',2'-c:4',5'-c']dithiophene-4,8-dione)], denoted

PBDB-T-SF, and the small molecule acceptor 3,9-bis(2-methylene-((3-(1,1-dicyanomethylene)-6,7-difluoro)-indanone))-5,5,11,11-tetrakis(4-hexylphenyl)-dithieno[2,3-d:2',3'-d']-s-indaceno[1,2-b:5,6-b']dithiophene, denoted IT-4F, were purchased from Solarmer Energy Inc. Appropriate donor:acceptor ratios were dissolved in chlorobenzene (Merck KGaA) with 0.25 vol% 1,8-DIO (Carl Roth GmbH) as solvent additive. The 7 mg mL<sup>-1</sup> solution was stirred at 100 °C for 24 h before slot-die coating the active layer. ITO-coated substrates (SOLEMS S.A., 12 Ω sq<sup>-1</sup> sheet resistance, 7.5 cm × 2.5 cm) were sequentially ultrasonic cleaned for 20 min with Alconox (Merck KGaA), deionized water, acetone (Merck KGaA), and isopropanol (Merck KGaA) and plasma treated for 10 min (Plasma-System-Nano, Diener Electronic GmbH, 0.4 mbar, O<sub>2</sub>, 83% power). Zink acetate dehydrate (1 g) (Merck KGaA) was dissolved in 10 mL 2-methoxyethanol (Merck KGaA) and 284 μL ethanolamine (Merck KGaA) and stirred for 8 h at room temperature. This precursor solution was spin-coated (5000 rpm, 60 s) on the ITO-coated glass substrates. After annealing at 200 °C for 60 min in air, the substrates were cooled down to room temperature before thin-film deposition. Meniscus-guided slot-die coating was performed at ambient conditions and room temperature with a flow rate of 10 μL s<sup>-1</sup>, a printing velocity of 10 mm s<sup>-1</sup>, and a height (distance between printer head and substrate) of 1 mm to achieve a dry film thickness of (100 ± 15) nm. After printing, the samples were cut into slices (2.5 × 2.5) cm<sup>2</sup> and transferred into a N<sub>2</sub>-filled glove box. Thin layers of MoO<sub>3</sub> (10 nm, Carl Roth GmbH) and Al (100 nm, chemPUR) were thermally evaporated under vacuum conditions (10<sup>-5</sup> mbar). The solar cells were transported to the synchrotron source in sealed, non-transparent containers filled with N<sub>2</sub> to avoid degradation by oxygen, air humidity, or ambient light.

**Setup and Measurement Conditions:** Printed organic photovoltaics based on PBDB-T-SF:IT-4F with a device area of 2.5 cm × 2.5 cm and a pixel size of 0.12 cm<sup>2</sup> were used without encapsulation. The devices were inserted into a vacuum chamber (10<sup>-2</sup> mbar) to exclude degradation by oxygen and air humidity. The chamber walls were cooled with water (15 °C) to avoid a temperature-induced decrease in the solar cell performance.

**Grazing Incidence Small Angle X-Ray Scattering:** GISAXS was performed at the MiNaXS beamline P03 at the PETRA III synchrotron source at DESY, Hamburg.<sup>[61]</sup> Measurements were carried out with a wavelength of 0.10642 nm and a sample-detector distance of 5262 mm. The incidence angle was aligned to 0.4° before the scattering experiment. A Pilatus 1 M detector (Dectris Ltd.) with a pixel size of 172 × 172 μm<sup>2</sup> was used for detecting the GISAXS signal. Oversaturation of the detector was avoided by a beamstop applied at the specular beam position. In operando, GISAXS was performed at one fixed position on the active layer close to the electrodes to avoid scattering contributions from the metal contacts. Measurements of 0.1 s were performed after 0, 2, 5, 15, 30, 60, 90, 140, 190, and 240 min of operation. Tests on radiation damage were done for each solar cell to rule out this problem for all systems studied (Figure S6, Supporting Information). Scattering data were analyzed and calibrated (sample-detector distance, beam center) using an open source Python program named Directly Programmable Data Analysis Kit (DPDAK).<sup>[62]</sup> Horizontal line cuts were carried out at the critical angle of PBDB-T-SF, which was calculated to be 0.12° for the applied X-ray energy of 11.65 keV.

**Current–Voltage Characterization:** Current–voltage curves were recorded every 20 s with a SourceMeter Keithley 2400 under AM1.5 illumination (100 mW cm<sup>-2</sup>). To record average J–V characteristics with high statistical significance, four solar cell pixels close to the GISAXS measurement position were connected in parallel. For the organic solar cell based on a 1:1 donor:acceptor ratio, the initial PCE was 2.3%. The device based on a donor:acceptor ratio of 1:2 achieved a PCE of 4.5% at the start of the device operation.

## Supporting Information

Supporting Information is available from the Wiley Online Library or from the author.

## Acknowledgements

The authors acknowledge funding from Deutsche Forschungsgemeinschaft (DFG, German Research Foundation) via International Research Training Group 2022 Alberta/Technical University of Munich International Graduate School for Environmentally Responsible Functional Materials (ATUMS) and under Germany's Excellence Strategy—EXC 2089/1—390776260 (e-conversion) and as well as from TUM.solar in the context of the Bavarian Collaborative Research Project Solar Technologies Go Hybrid (SolTech) and the Center for NanoScience (CeNS). K.S.W. acknowledges funding by the Hans Böckler Stiftung and W.C., S.Y., and R.G. by the China Scholarship Council (CSC). In operando, GISAXS experiments were carried out at the light source PETRA III at DESY, a member of the Helmholtz Association (HGF).

## Conflict of Interest

The authors declare no conflict of interest.

## Keywords

degradation mechanisms, meniscus-guided slot-die coatings, organic solar cells, short-circuit currents

Received: May 16, 2020  
Published online: June 8, 2020

- [1] Q. An, X. Ma, J. Gao, F. Zhang, *Sci. Bull.* **2019**, *64*, 504.
- [2] B. Fan, D. Zhang, M. Li, W. Zhong, Z. Zeng, L. Ying, F. Huang, Y. Cao, *Sci. China Chem.* **2019**, *62*, 746.
- [3] C. N. Hoth, P. Schilinsky, S. A. Choulis, C. J. Brabec, *Nano Lett.* **2008**, *8*, 2806.
- [4] C. N. Hoth, S. A. Choulis, P. Schilinsky, C. J. Brabec, *Adv. Mater.* **2007**, *19*, 3973.
- [5] F. C. Krebs, *Sol. Energy Mater. Sol. Cells* **2009**, *93*, 394.
- [6] T. M. Eggenhuisen, Y. Galagan, A. F. K. V. Biezemans, T. M. W. L. Slaats, W. P. Voorthuizen, S. Kommeren, S. Shanmugam, J. P. Teunissen, A. Hadipour, W. J. H. Verhees, S. C. Veenstra, M. J. J. Coenen, J. Gilot, R. Andriessen, W. A. Groen, *J. Mater. Chem. A* **2015**, *3*, 7255.
- [7] J. Chang, C. Chi, J. Zhang, J. Wu, *Adv. Mater.* **2013**, *25*, 6442.
- [8] F. Liu, S. Ferdous, E. Schaible, A. Hexemer, M. Church, X. Ding, C. Wang, T. P. Russell, *Adv. Mater.* **2015**, *27*, 886.
- [9] S. Pröller, F. Liu, C. Zhu, C. Wang, T. P. Russell, A. Hexemer, P. Müller-Buschbaum, E. M. Herzig, *Adv. Energy Mater.* **2016**, *6*, 1501580.
- [10] X. Gu, L. Shaw, K. Gu, M. F. Toney, Z. Bao, *Nat. Commun.* **2018**, *9*, 534.
- [11] C. Giroto, D. Moia, B. P. Rand, P. Heremans, *Adv. Funct. Mater.* **2011**, *21*, 64.
- [12] D. Vak, S.-S. Kim, J. Jo, S.-H. Oh, S.-I. Na, J. Kim, D.-Y. Kim, *Appl. Phys. Lett.* **2007**, *91*, 81102.
- [13] S. M. McAfee, S. V. Dayneko, P. Josse, P. Blanchard, C. Cabanetos, G. C. Welch, *Chem. Mater.* **2017**, *29*, 1309.
- [14] S. Holliday, R. S. Ashraf, A. Wadsworth, D. Baran, S. A. Yousaf, C. B. Nielsen, C.-H. Tan, S. D. Dimitrov, Z. Shang, N. Gasparini, M. Alamoudi, F. Laquai, C. J. Brabec, A. Salleo, J. R. Durrant, I. McCulloch, *Nat. Commun.* **2016**, *7*, 11585.
- [15] H. J. Son, W. Wang, T. Xu, Y. Liang, Y. Wu, G. Li, L. Yu, *J. Am. Chem. Soc.* **2011**, *133*, 1885.

- [16] X. Du, T. Heumueller, W. Gruber, A. Classen, T. Unruh, N. Li, C. J. Brabec, *Joule* **2019**, 3, 215.
- [17] W. Wang, C. J. Schaffer, L. Song, V. Körstgens, S. Pröller, E. D. Indari, T. Wang, A. Abdelsamie, S. Bernstorff, P. Müller-Buschbaum, *J. Mater. Chem. A* **2015**, 3, 8324.
- [18] B. Zimmermann, U. Würfel, M. Niggemann, *Sol. Energy Mater. Sol. Cells* **2009**, 93, 491.
- [19] M. Jørgensen, K. Norrman, F. C. Krebs, *Sol. Energy Mater. Sol. Cells* **2008**, 92, 686.
- [20] Z. He, C. Zhong, S. Su, M. Xu, H. Wu, Y. Cao, *Nat. Photonics* **2012**, 6, 591.
- [21] Q. L. Song, M. L. Wang, E. G. Obbard, X. Y. Sun, X. M. Ding, X. Y. Hou, C. M. Li, *Appl. Phys. Lett.* **2006**, 89, 251118.
- [22] C. J. Schaffer, C. M. Palumbiny, M. A. Niedermeier, C. Jendrzewski, G. Santoro, S. V. Roth, P. Müller-Buschbaum, *Adv. Mater.* **2013**, 25, 6760.
- [23] D. Yang, F. C. Löhner, V. Körstgens, A. Schreiber, S. Bernstorff, J. M. Buriak, P. Müller-Buschbaum, *ACS Energy Lett.* **2019**, 4, 464.
- [24] C. J. Schaffer, C. M. Palumbiny, M. A. Niedermeier, C. Burger, G. Santoro, S. V. Roth, P. Müller-Buschbaum, *Adv. Energy Mater.* **2016**, 6, 1600712.
- [25] P. Cheng, X. Zhan, *Chem. Soc. Rev.* **2016**, 45, 2544.
- [26] S. A. Gevorgyan, N. Espinosa, L. Ciannaruchi, B. Roth, F. Livi, S. Tsopanidis, S. Züfle, S. Queirós, A. Gregori, G. A. D. R. Benatto, M. Corazza, M. V. Madsen, M. Hösel, M. J. Beliatas, T. T. Larsen-Olsen, F. Pastorelli, A. Castro, A. Mingorance, V. Lenzi, D. Fluhr, R. Roesch, M. Maria Duarte Ramos, A. Savva, H. Hoppe, L. S. A. Marques, I. Burgués, E. Georgiou, L. Serrano-Luján, F. C. Krebs, *Adv. Energy Mater.* **2016**, 6, 1600910.
- [27] G. Dennler, C. Lungenschmied, H. Neugebauer, N. S. Sariciftci, M. Latrèche, G. Czeremuszkin, M. R. Wertheimer, *Thin Solid Films* **2006**, 511–512, 349.
- [28] W. Zhao, S. Li, H. Yao, S. Zhang, Y. Zhang, B. Yang, J. Hou, *J. Am. Chem. Soc.* **2017**, 139, 7148.
- [29] J. Hou, O. Inganäs, R. H. Friend, F. Gao, *Nat. Mater.* **2018**, 17, 119.
- [30] C. Fan, *Probing Organic Solar Cells with Grazing Incidence Scattering Techniques*, Wiley-VCH Verlag GmbH & Co. KGaA, Weinheim **2018**.
- [31] P. Müller-Buschbaum, *Adv. Mater.* **2014**, 26, 7692.
- [32] A. Hexemer, P. Müller-Buschbaum, *IUCr* **2015**, 2, 106.
- [33] A. Seemann, T. Sauermann, C. Lungenschmied, O. Armbruster, S. Bauer, H.-J. Egelhaaf, J. Hauch, *Sol. Energy* **2011**, 85, 1238.
- [34] K. Norrman, S. A. Gevorgyan, F. C. Krebs, *ACS Appl. Mater. Interfaces* **2009**, 1, 102.
- [35] M. Hermenau, M. Riede, K. Leo, S. A. Gevorgyan, F. C. Krebs, K. Norrman, *Sol. Energy Mater. Sol. Cells* **2011**, 95, 1268.
- [36] M. Wang, F. Xie, J. Du, Q. Tang, S. Zheng, Q. Miao, J. Chen, N. Zhao, J. B. Xu, *Sol. Energy Mater. Sol. Cells* **2011**, 95, 3303.
- [37] H. B. Yang, Q. L. Song, C. Gong, C. M. Li, *Sol. Energy Mater. Sol. Cells* **2010**, 94, 846.
- [38] Y. Jiang, L. Sun, F. Jiang, C. Xie, L. Hu, X. Dong, F. Qin, T. Liu, L. Hu, X. Jiang, Y. Zhou, *Mater. Horiz.* **2019**, 6, 1438.
- [39] P. Schilinsky, C. Waldauf, J. Hauch, C. J. Brabec, *J. Appl. Phys.* **2004**, 95, 2816.
- [40] L. J. A. Koster, V. D. Mihailetschi, R. Ramaker, P. W. M. Blom, *Appl. Phys. Lett.* **2005**, 86, 123509.
- [41] B. Conings, S. Bertho, K. Vandewal, A. Senes, J. D'Haen, J. Manca, R. A. J. Janssen, *Appl. Phys. Lett.* **2010**, 96, 163301.
- [42] B. Ray, M. A. Alam, *Appl. Phys. Lett.* **2011**, 99, 33303.
- [43] S. Schuller, P. Schilinsky, J. Hauch, C. J. Brabec, *Appl. Phys. A* **2004**, 79, 37.
- [44] P. Müller-Buschbaum, *Anal. Bioanal. Chem.* **2003**, 376, 3.
- [45] M. Stamm, *Polymer Surfaces and Interfaces*, Springer, Berlin, Heidelberg **2008**.
- [46] M. Gomez, A. Nogales, M. C. Garcia-Gutierrez, T. A. Ezquerra, *Applications of Synchrotron Light to Scattering and Diffraction in Materials and Life Sciences*, Springer, Berlin, Heidelberg **2009**.
- [47] C. J. Schaffer, J. Schlipf, E. Dwi Indari, B. Su, S. Bernstorff, P. Müller-Buschbaum, *ACS Appl. Mater. Interfaces* **2015**, 7, 21347.
- [48] M. A. Ruderer, S. Guo, R. Meier, H.-Y. Chiang, V. Körstgens, J. Wiedersich, J. Perlich, S. V. Roth, P. Müller-Buschbaum, *Adv. Funct. Mater.* **2011**, 21, 3382.
- [49] S. Guo, W. Wang, E. M. Herzig, A. Naumann, G. Tainter, J. Perlich, P. Müller-Buschbaum, *ACS Appl. Mater. Interfaces* **2017**, 9, 3740.
- [50] K. S. Wienhold, V. Körstgens, S. Grott, X. Jiang, M. Schwartzkopf, S. V. Roth, P. Müller-Buschbaum, *ACS Appl. Mater. Interfaces* **2019**, 11, 42313.
- [51] X. Du, T. Heumueller, W. Gruber, O. Almora, A. Classen, J. Qu, F. He, T. Unruh, N. Li, C. J. Brabec, *Adv. Mater.* **2020**, 32, e1908305.
- [52] A. J. Heeger, *Adv. Mater.* **2014**, 26, 10.
- [53] H. Hoppe, N. S. Sariciftci, *J. Mater. Chem.* **2006**, 16, 45.
- [54] N. Kaur, M. Singh, D. Pathak, T. Wagner, J. M. Nunzi, *Synth. Met.* **2014**, 190, 20.
- [55] P. W. M. Blom, V. D. Mihailetschi, L. J. A. Koster, D. E. Markov, *Adv. Mater.* **2007**, 19, 1551.
- [56] Y. Liu, J. Zhao, Z. Li, C. Mu, W. Ma, H. Hu, K. Jiang, H. Lin, H. Ade, H. Yan, *Nat. Commun.* **2014**, 5, 5293.
- [57] H. Yan, S. Swaraj, C. Wang, I. Hwang, N. C. Greenham, C. Groves, H. Ade, C. R. McNeill, *Adv. Funct. Mater.* **2010**, 20, 4329.
- [58] B. A. Collins, Z. Li, J. R. Tumbleston, E. Gann, C. R. McNeill, H. Ade, *Adv. Energy Mater.* **2013**, 3, 65.
- [59] I. A. Howard, R. Mauer, M. Meister, F. Laquai, *J. Am. Chem. Soc.* **2010**, 132, 14866.
- [60] C. M. Proctor, M. Kuik, T.-Q. Nguyen, *Prog. Polym. Sci.* **2013**, 38, 1941.
- [61] A. Buffet, A. Rothkirch, R. Döhrmann, V. Körstgens, M. M. Abul Kashem, J. Perlich, G. Herzog, M. Schwartzkopf, R. Gehrke, P. Müller-Buschbaum, S. V. Roth, *J. Synchrotron Radiat.* **2012**, 19, 647.
- [62] G. Benecke, W. Wagermaier, C. Li, M. Schwartzkopf, G. Flucke, R. Hoerth, I. Zizak, M. Burghammer, E. Metwalli, P. Müller-Buschbaum, M. Trebbin, S. Förster, O. Paris, S. V. Roth, P. Fratzl, *J. Appl. Crystallogr.* **2014**, 47, 1797.